Surface finish has a critical influence on biofilm formation and mammalian cell attachment to additively manufactured prosthetics

Cox, Sophie; Jamshidi, Parastoo; Eisenstein, Neil; Webber, Mark; Burton, Hanna; Moakes, Richard; Addison, Owen; Attallah, Moataz; Shepherd, Duncan; Grover, Liam

DOI:
10.1021/acsbiomaterials.7b00336

Document Version
Peer reviewed version

Citation for published version (Harvard):
Cox, S, Jamshidi, P, Eisenstein, N, Webber, M, Burton, H, Moakes, R, Addison, O, Attallah, M, Shepherd, D & Grover, L 2017, 'Surface finish has a critical influence on biofilm formation and mammalian cell attachment to additively manufactured prosthetics', *ACS Biomaterial Science and Engineering*, vol. 3, no. 8, pp. 1616-1626. https://doi.org/10.1021/acsbiomaterials.7b00336

Surface Finish has a Critical Influence on Biofilm Formation and Mammalian Cell Attachment to Additively Manufactured Prosthetics

Sophie C. Cox[1*], Parastoo Jamshidi[2], Neil M. Eisenstein[1,3], Mark A. Webber[4,5], Hanna Burton[1,6], Richard J. A. Moakes[1], Owen Addison[6], Moataz Attallah[2], Duncan E.T. Shepherd[7], Liam M. Grover[1]

[1]School of Chemical Engineering, University of Birmingham, Edgbaston, B15 2TT, UK

[2]School of Materials and Metallurgy, University of Birmingham, Edgbaston, B15 2TT, UK

[3] Royal Centre for Defence Medicine, Birmingham Research Park, Vincent Drive, Edgbaston B15 2SQ, UK

[4]Institute of Microbiology and Infection, University of Birmingham, Edgbaston, B15 2TT, UK

[5]Institute of Food Research, Norwich Research Park, Norwich, NR4 7UA

[6]School of Dentistry, University of Birmingham, Edgbaston, B15 2TT, UK

[7]Department of Mechanical Engineering, School of Engineering, University of Birmingham, Edgbaston, B15 2TT, UK

*Corresponding author, telephone +44(0)1214145351, s.c.cox@bham.ac.uk

Abstract

Additive manufacturing (AM) technologies enable greater geometrical design freedom compared with subtractive processes. This flexibility has been used to manufacture patient-matched implants. Whilst the advantages of AM are clear, the optimisation at each process stage is often understated. Here we demonstrate that surface finishing of selective laser melted (SLM) implants significantly alters topography, which has implications for cellular and biofilm adhesion.

Hot isostatic pressing of as-fabricated Ti-6Al-4V implants was shown to reduce porosity (1.04 to 0.02%) and surface roughness (34±8 to 22±3μm). Despite these surface changes, pre-osteoblasts exhibited a similar viability and proliferation after 7 days of culture. Contrastingly, sandblasting and polishing significantly reduced cellular activity and increased cytotoxicity. Bacterial specimens (S*taphylococcus aureus, Staphylococcus epidermidis* and *Pseudomonas aeruginosa*) adhered more homogenously to sandblasted implants compared with other treatments. This suggests that sandblasting may place the implant at risk of infection and reduce the strength of interaction with the surrounding soft tissues.

The ability to tune the adhesion of cells to additively manufactured Ti-6Al-4V implants using post-processing methods was demonstrated. Since the degree of tissue integration required of implants is application specific, these methods may be useful to tailor osseointegration. However, surface competition between mammalian and bacterial cells remains a challenge.

Keywords: Additive manufacture, Selective Laser Melting, Surface Finishing, Cell adhesion, biofilm

1.0 Introduction

Since the invention of stereolithography in the 1980s, additive manufacturing (AM) technologies have developed rapidly and numerous techniques are now available that use a range of different substrate materials [1, 2]. A major advantage of AM over subtractive methods is the improved degree of geometrical freedom made possible through manufacture of the part layer-by-layer. The ability to manufacture customised parts, gradient structures, and internal features using AM is an attractive concept to many industries, including medical, automotive, and aerospace.

There is a clinical need for patient bespoke implants, particular in anatomical regions that vary significantly between patients, which has led to a surge in the development of subtractive and AM technologies for customised implant manufacture [3-5]. In recent years the ability of AM to add further value to such prostheses has begun to be realised. For example, tailoring of the implant surface to facilitate osseointegration [6, 7], lattice structure optimisation to minimise stress shielding [8, 9], and manipulation of implant geometry to enable incorporation of therapeutically loaded materials [10].

While the advantages of AM are clearly presented, the complexities and optimisation required for both the fabrication and post-manufacturing processes associated with production of parts are often understated. The general process chain for AM typically involves: 1) 3-dimensional computer aided design (CAD) modelling, 2) standard triangulation language (STL) file generation, 3) file verification and repair, 4) build file creation, 5) part construction, and 6) part cleaning and finishing [11]. To fabricate metallic implants (stainless steels, cobalt chromium molybdenum alloys, and titanium alloys) laser based AM systems are typically used. These include, selective laser sintering [12, 13], selective laser melting (SLM) [10, 14-16], and electron beam melting [8, 17]. In each of these techniques a different mechanism is used to fuse the metallic powder particles together. For SLM the thermal energy of the laser beam is used to melt the particles, which then consolidate to form the part geometry. This process is conducted layer-by-layer in an inert atmosphere to prevent oxidation of the metals. Since the part is

surrounded by unconsolidated powdered stock material during building it is necessary to manufacture support structures, which prevent collapse during the build.

Post-fabrication, the support structures must be removed, usually by machining or wire cutting. It may also be necessary to conduct post-fabrication processing to address inherent issues associated with the AM process, and/or tailor the performance of the part to the intended application. Common issues associated with metallic SLM parts include: cracking, porosity, residual stresses, columnar grain structure, rough surface topography, and anisotropy in mechanical properties [18]. As such, processes such as hot isostatic pressing (HIPing) are routinely used in industrial AM applications to reduce bulk porosity by simultaneously applying high temperature and pressure [19]. A number of studies have considered the effects of HIPing on the mechanical performance of metallic SLM parts, including Ti-6Al-4V and Ni-superalloys [18-20]. Qiu *et al.* demonstrated a transformation from martensitic structures into α and β phases after HIPing of Ti-6Al-4V parts manufactured by SLM. This microstructural change resulted in a notable improvement in ductility but a reduction in tensile strength [18] and the fatigue performance of AM parts has been shown to be poor compared with rolled equivalents [21]. Therefore surface-processing techniques, such as sand blasting or polishing may be required after HIPing to remove partially melted precursor particles and reduce surface roughness. In addition to affecting the mechanical performance of implants, changes in surface topography may also influence mammalian and bacterial cell adhesion and proliferation, as well as biofilm formation [22-24].

In this paper Ti-6Al-4V parts were manufactured by SLM and post-processed by HIPing, sandblasting, and polishing. The topography of all surfaces was observed by scanning electron microscopy (SEM) and micro-computed tomography. White light interferometry was also used to quantify the average surface roughness (S_a). Here, a comparison of the adhesion and proliferation of pre-osteoblast cells (MC3T3), and three bacterial organisms commonly associated with orthopaedic infections (*Staphylococcus aureus*, *Staphylococcus epidermidis*, and *Pseudomonas aeruginosa*) was observed on as-fabricated and post-processed surfaces. Confocal microscopy and quantitative *in-vitro* assays

were used to demonstrate significant variations in cellular viability, metabolic activity and cytotoxicity. In summary, this work reveals some important considerations regarding the implementation of AM implants for hard tissue applications.

2.0 Materials and Methods

2.1 Selective laser melting of Ti-6Al-4V implant models

Two designs of cylinders (Fig. 1a) were used to produce implant models. A hole was introduced into the cylinder to mimic a typical design feature that may be found on an implant, e.g. for the purpose of fixation or filling of the implant with a secondary material containing a therapeutic entity [10]. These two designs were consider to assess whether additional features may affect the surface properties and, in turn, cellular adhesion properties of parts additively manufactured using selected laser melting (SLM). The implant models using the same method and process parameters as our previous study [25]. Briefly, cylinders were fabricated from Ti-6Al-4V gas atomised powder (TLS, Technik, Germany) sized 20-50 µm using a M2 Cusing® SLM system (Concept Laser, Germany), which employs an Nd:YAG laser. This system operates an island scanning strategy in which the build is divided into a number of square 'islands' (see [18] or schematic in Figure 4a). The islands are scanned randomly and the scan direction is rotated 90° between neighbouring islands [18]. The parameters used to fabricate cylinders were 150 W laser power, 1750 mm/s scanning speed, 20 µm slice thickness, and hatch spacing of 75 µm. Support structures were built between the substrate base and each individual implant to provide stability during the build. Manufacture was conducted in a chamber flooded with argon gas to minimise oxygen pick-up to < 0.1%.

As-fabricated (AF) parts were then processed using HIPing (referred to as HIP in figures). Following HIPing, samples were further modified by sandblasting (SB) or polishing (P). SB and P were applied to remove residual partially melted powder particles and reduce surface roughness.

2.1.1 Post-processing of the SLMed parts

HIPing was performed using an EPSI HIPping vessel (Temse, Belgium). Samples were HIPped as per ASTM F3001-14 (*Standard Specification for Additive Manufacturing Ti-6Al-4V ELI (Extra Low Interstitial) with Power Bed Fusion*) at 930°C/ 100 MPa/ 4 h, followed by cooling at a rate of 5°C/min. SB was performed in an Air Blast cabinet (CBI Equipment Ltd, UK) using a blasting gun with a compressed air regulator set to 4 bar. CARBOREX micro grit black abrasive powder with a size of 53 µm was used for SB (Washington Mill Electro Minerals, UK). The grit blasting was performed for 30 minutes with a speed of 100 m/s. SB is a commonly used as a standard procedure in industrial SLM operations to improve the surface finish, it was applied to remove the residual partially melted particle powder on the surface. The polishing process was performed using a centrifugal disc finishing machine (Finishing Techniques Ltd, FINTEK). This is a 2-stages wet polishing process, using first aluminium oxide balls (6-10 mm), followed by plastic grinding chips (6-10 mm) as the media to deburr and polish the parts, with total process duration of 7 hours. All parts were cleaned using compressed air, an ultrasonic bath, and isopropyl alcohol. Further cleaning was also undertaken before biological tests to sterilise the parts (Section 2.3).

2.2 Characterisation of additively manufactured parts

2.2.1 Visualisation of surface topography using scanning electron microscopy

Secondary electron images of Ti-6Al-4V specimens were obtained using a XL30 FEG environmental SEM (Philips, UK) operating at 20 kV. Prior to imaging, samples were attached to an aluminium stub using double adhesive carbon tabs.

2.2.2 3-dimensional visualisation and porosity analysis using micro-computed tomography

As-fabricated and surface treated parts were scanned using a Skyscan1172 micro-computed tomography (micro-CT) system (Bruker, Belgium) with 80 kV maximum X-ray energy, 8 W beam power, 1650 ms exposure per projection, aluminium and copper filter, and 7.98 µm pixel size. Reconstructed data were visualised in 3D using *CTVox* (version 3.0, Bruker) software. A porosity analysis was

conducted using *CTAn* (version 1.15.4.0, Bruker) software. Briefly, a circle was fitted to the external edges of the sample to create a region of interest (ROI). This ROI was interpolated across 200 slices positioned in the middle of the sample volume (z-axis) to create a volume of interest (VOI). A global thresholding was applied to create a binary image, which was then filtered to remove noise. 3D analysis was run over this VOI to determine total porosity as well as the size distribution of pores.

2.2.3 3-dimensional surface reconstruction using optical microscopy

Optical imaging of as-fabricated and surface treated parts was performed using an Alicona microscope (G5 Infinite Focus, Alicona UK, Kent, UK) at ×20 magnification. At the central point of the surface, an area of 1 mm by 1 mm was scanned. Scanning was performed between the maximum and minimum focussing points of the z height of each sample surface. A 3D surface was reconstructed using the Alicona IF-Laboratory Measurement Module (version 6.1, Alicona UK, Kent, UK).

2.2.4 Quantification of arithmetic mean height

A MicroXAM interferometer (KLA Tencor, UK) operating a white light source was used to profile the surface of Ti-6Al-4V SLM surface for all treatments. Scanning Probe Image Processor software (Image Metrology, Denmark) was employed for the analysis of acquired images yielding arithmetical mean height surface roughness values (S_a). Three measurements (0.6 x 0.8 mm) were obtained at locations representative of the overall surface for three different samples without designed surface holes (Figure 1a). Measurements of three separate samples with holes were obtained from the periphery of the hole diameter to ascertain whether the topography in this location was different from the rest of the surface (n=3). In total 9 measurements (3 measurements of 3 different samples) were taken for each sample variant and results presented as mean ± standard error of the mean.

Single factor analysis of variance (ANOVA) tests were conducted to assess any significance within groups (i.e. between samples of the same treatment and design). This was used as an assessment of reproducibility. A two-way ANOVA with factors as: surface condition at four levels (as-fabricated, HIP,

HIP+SB and HIP+P) and presence or absence of a hole (at 2 levels) with post-hoc Tukey tests was conducted to determine if surface treatments significantly altered Sa. Statistical tests were performed at $\alpha = 0.05$ using SPSS Statistics (v24, IBM).

2.2.5 Contact angle

Contact angle measurements were obtained using an image capture followed by a droplet fitting method. Samples (Figure 1) were place on a flat surface and deionised water (7 μm) pipetting into the centre. Images were captured across the horizontal plane of the droplet 60 seconds after application. An image processing package (Image J) was used to undertake analysis using a Low-Bond Axisymmetric Drop Shape Analysis (LB-ADSA) plugin [26]. Images were converted to 8-bit greyscale and cropped to the droplet area. LB-ADSA was applied ensuring good fitting to the droplet and contact angle obtained as the inner angle between the surface and air/water interface.

2.3 In-vitro adhesion and proliferation of MC3T3 pre-osteoblast cells

The base medium used for in-vitro work was Alpha Minimum Essential Media (α-MEM) with sodium bicarbonate, ribonucleosides and deoxyribonucleosides (M426, Sigma, UK). Complete growth media was made by supplementing α-MEM media with a final concentration of 10% fetal bovine serum (F7524, Sigma, UK), 2.4% l-glutamine (G7513, Sigma, UK) and 1% penicillin-streptomycin (F4333, Sigma, UK). MC3T3-E1 preosteoblast cells (Subclone 4, CRL-2593, ATCC, USA) were cultured in complete growth media as per supplier instructions. Prior to in-vitro experiments, samples were autoclaved, washed with 100% ethanol, and left overnight under ultra-violet light.

For all assays, aliquots of MC3T3-E1 cells ($1x10^4$ cells/cm^2) were seeded on to the top surface of AM samples and tissue culture plastic as a control. Cells were allowed to adhere for 2 hours and after this time complete growth media was added to each well to cover the sample surface. Cultures were incubated in 5% CO_2 atmosphere maintained at 37°C.

2.3.1 Cell viability

The viability of cells after culturing for 1, 3, and 7 days were analysed by staining with calcein-AM (1 mg/mL, Molecular Probes, UK) and propidium iodide (1 mg/mL, Invitrogen, UK). Calcein-AM is a green florescent dye that is cell-permeant and converts into intense fluorescent calcein by the activity of an intracellular esterase, an enzyme found in live cells [27]. Propidium iodide is membrane impermeable and is excluded from viable cells. It binds to DNA by intercalating between base pairs. Stained cultures were visualised using a scanning confocal microscope (Olympus FV1000, Multiple Ar laser, Germany) and typical images collected for two samples of each variant.

2.3.2 Cell proliferation and cytotoxicity

Alamar blue (Invitrogen, UK) was used as a non-invasive proliferation assay and was performed on days 1, 3, and 7. Alamar blue is a redox indicator that yields a colorimetric change and fluorescent signal in response to metabolic activities. Briefly, culture medium was removed from samples and stored for cytotoxicity testing. Fresh media containing 10v% Alamar blue dye was then added and the plates were placed in an incubator at 37°C for 4 h. After this time, 200 µL from each well was transferred to a 96-well plate and colorimetric change was analysed using a GloMax®-Multi spectrometer (Promega Corporation, UK) at 530-560 nm excitation and 590 nm emission. This assay was conducted in triplicate.

A lactate dehydrogenase (LDH) assay kit (Thermo Scientific™ Pierce™, UK) was used to quantify cellular cytotoxicity. LDH is a cytosolic enzyme that can be released into cell culture media as a result of plasma membrane damage. Therefore quantification of LDH in culture media is indicative of cytotoxicity. The assay was conducted according to supplier protocols after 1, 3, and 7 days of culture on triplicate samples. Briefly, 50 µL culture media was removed from metallic samples used for Alamar blue assay at each time point, transferred to a 96-well plate and mixed with 50 µL Reaction Mixture. After incubation at 20°C for 30 minutes reactions were stopped by adding Stop Solution and absorbance at 490 and 680 nm was measured using a GloMax®-Multi spectrometer.

At each time-point and one-way ANOVAs and post-hoc Tukey tests ($\alpha = 0.05$) were conducted to determine if the different surface treatments significantly altered metabolic activity or cytotoxicity including comparison to the control tissue culture plastic samples.

2.4 Bacterial adhesion

The ability of *Staphylococcus aureus* (NCTC 8532), *Staphylococcus epidermidis* (NCTC 11047), and *Pseudomonas aeruginosa* (NCTC 10662) to adhere to Ti-6Al- 4V surfaces was quantitatively assessed using crystal violet staining. This assay provided non-spatially specific quantification of bacterial adhesion across all surfaces of the cylindrical samples (i.e. top faces and curved circumference). Metallic samples (Figure 1a) were sterilised in 100% ethanol and allowed to dry before being placed in 30 mL sterile polypropylene universal tubes (n=3 for each culture). Into each tube, 10 mL of Lysogeny broth (LB - Sigma Aldrich, UK) that had been inoculated 1:100 (i.e. with 100 µl) of an overnight culture (also in LB) was then added. Samples were incubated at 37°C with shaking at 25 rpm for 48 hours to allow for saturated growth in the bacterial culture. After incubation, the metallic samples were removed from the media and washed to remove any non-adherent cells. Samples were then immersed in 1 ml of 1 % (w/v) crystal violet (CV) solution for 10 minutes. Any unbound dye was removed by washing samples with deionised water and each sample was then transferred and immersed in 70% ethanol to solubilise bound CV. The samples were removed and the absorbance of the remaining liquid from each sample was measured. Three absorbance readings at 600 nm were obtained from each replicate using a FluoSTAR Optima plate reader (BMG Labtech). Independent student's t-tests were conducted to determine if surface treatments significantly altered the adhesion of bacterial cultures. For each culture, equivalent sample designs of as-fabricated groups were compared with HIP samples, and HIP alone was compared with HIP + SB as well as HIP + P. Statistical tests were performed at $\alpha = 0.05$.

Initial adhesion of bacterial cells on SLM samples were visualised using a live/dead staining kit (ThermoFisher Scientific, UK). Overnight cultures of *Staphylococcus aureus*, *Staphylococcus*

epidermidis, and *Pseudomonas aeruginosa* in LB were diluted to an optical density of 0.06 (600 nm). Ti-6Al-4V samples were sterilised in 100% ethanol, allowed to dry, placed in 24-well plates and covered in diluted LB cultures. Plates were incubated at 37°C with shaking at 25 rpm for 3 hours. After this time SYTO® 9 and propidium iodide dyes were added to stain live and dead cells, respectively according to manufacturer's instructions. Images were obtained of the flat top face of all surface treatments using a scanning confocal microscope (Olympus FV1000, Multiple Ar laser, Germany). This assay was conducted in duplicate with tissue culture plastic (TCP) as a control.

3.0 Results

3.1 Surface topography

Scanning electron micrographs and 3D micro-CT reconstructions revealed the island scanning strategy used to manufacture parts (Figures 2 and 3). Spherical partially-melted powder particles were observed on the flat-top surface of AF and HIP samples (Figure 2). Pores, located in both the troughs and peaks of the island patterning, were visualised on AF specimens but were not seen after HIP was performed. HIP + SB and HIP + P samples exhibited notably different surface topographies compared to AF and HIP surfaces. The island scanning strategy was still distinguishable on HIP + SB surfaces; however, polishing was shown to remove the majority of these channels. No partially melted powder particles were observed after SB or P. Furthermore, the top face of equivalent samples with and without holes were indistinguishable. However, a greater number of partially melted particles were present on the circumference-face of equivalent samples with holes (Figure 2b).

On micro-CT analysis, some samples revealed peaks across their whole width that were not part of the island pattern strategy. These defects were observed on AF and HIP samples (Figure 3a). A notable difference in surface topography was observed as a result of sandblasting and polishing of HIP samples. The island patterning strategy was clearly observed for all samples except HIP + P where troughs and peaks of the tracks had been substantially reduced. Micro-CT analysis confirmed that HIP

substantially reduced sample porosity to 0.02% compared with AF samples (1.04%). Notably fewer pores >23.9 μm (three times scanning pixel size) were detected in HIP and HIP + SB samples compared with AF (Figure 3b). Interestingly, polished samples exhibited the highest fraction of pores sized 23.9 - <39.9 μm but no pores greater in size than this range. Notably the contact angle for HIP + SB was significantly lower (7.90 ± 1.65°) than AF (71.5 ± 19.1°), HIP (103.5 ± 25.5°), and HIP + P (58.6 ± 20.0°). This sample also exhibited the highest percentage of pores < 23.9 μm.

For each sample three measurements of S_a were obtained within different islands (Figure 4a). No significant difference ($p>0.05$) between measurements of samples prepared using the same treatment were observed (Figure 4b). This suggests that S_a was reproducible within treatment groups. Surface treatment significantly affected S_a ($p<0.001$) but the introduction of hole did not impact on the recorded S_a –value ($p=0.56$). HIPing was shown to significantly reduce the average S_a values for samples ($p<0.001$) with (21.8 ± 3.3 μm) and without (23.7 ± 3.7 μm) holes when compared with AF equivalents (33.6 ± 7.5 μm and 33.1 ± 6.2 μm, respectively) (Figure 4c). Sandblasting of HIPed samples led to a further significant reduction in S_a ($p<0.001$); 5.86 ± 1.70 μm with and 6.83 ± 1.71 μm without hole features. Polished surfaces exhibited the lowest S_a values of all the groups; 0.20 ± 0.07 μm and 0.16 ± 0.04 μm with and without hole features, respectively. This was shown to be significantly different from HIP and HIP + SB equivalents ($p<0.001$ for both with and without surface features).

3.2 In-vitro adhesion and proliferation of MC3T3 pre-osteoblast cells

MC3T3-E1 cells were observed to adhere to all Ti-6Al-4V surfaces after 1 day of culture. After 7 days on AF and HIP surfaces cells had migrated and proliferated across the whole sample surface area except for regions where partially melted particles were present (Figure 5a and b). Contrastingly, surfaces that were sandblasted or polished following HIP had significantly fewer adhered cells after 3 days of culture on samples with and without holes (Figure 5 c and d). Notably, a number of dead (red) MC3T3-E1 cells were observed on HIP + SB and HIP + P samples after 7 days of culture. Specifically, live cells (green) on polished surfaces were seen to be clustered together in small areas across the

surface and after 7 days migrated cells outside of these areas were largely dead. In general throughout this study, the morphology of live cells on HIP + SB samples were observed to be more rounded in comparison to cells seeded on tissue culture plastic as well as other Ti-6Al-4V treatment surfaces.

Notably after 7 days of culture, HIP + SB and HIP + P samples, both with and without holes, exhibited significantly lower ($p<0.01$) cellular metabolic activity compared with HIP alone (Figure 6). After only 24 hours MC3T3 cells adhered to sandblasted and polished samples were shown to elicit a significantly ($p<0.01$) higher metabolic activity compared with HIP. No significant ($p>0.05$) differences in Alamar Blue reduction between AF and HIP samples were noted throughout the experiment (Figure 6a and b). After 3 days of culture, cells seeded on tissue culture plastic demonstrated significantly higher metabolic activity compared with all metallic samples ($p<0.001$). Alongside this metabolic assay, cytotoxicity testing was conducted using a LDH kit (Figure 6c and d). The results of these two assays complement each other since significantly ($p<0.05$) higher levels of toxicity after 7 days were detected for HIP + SB and HIP + P samples compared with both hot isostatic pressing alone and controls for surfaces with (Figure 6c) and without holes (Figure 6d).

3.3 Bacterial adhesion

Crystal violet staining was used to assess the amount of biofilm formed on each Ti-6Al-4V surface after 48 hrs of culture (Figure 7a). This assay provided non-spatially specific information and few consistent trends were observed between the three tested cultures. Significantly ($p<0.05$) more bacteria was shown to adhere to AF and HIP + SB samples compared with HIPing alone in a number of cases (Figure 7a). Staining of samples allowed for adherent cells to be spatially located on the top flat surface of cylindrical samples (Figure 7b and c). In the case of samples that exhibited the island scanning topography (AF and HIP) all strains primarily aligned along the peaks either side of laser tracks. Some cells were seen to adhere in surface troughs of these samples, in particular for *Pseudomonas aeruginosa* (Figure 7c). The arrangement of bacterial cells on SB surface was notably more random compared with AF and HIP. Bacterial cells were demonstrated to adhere to polished surfaces in areas

that had not been sufficiently been smoothed down. Interestingly, in the case of *Pseudomonas aeruginosa,* notably more viable cells were found outside of these rough areas.

4.0 Discussion

For a manufacturing process to be adopted widely by industry, the repeatability and consistency of the produced parts are critical. The high temperature gradients and complex thermal history involved in laser-based AM methods, such as SLM, mean that optimisation is needed to guarantee material properties for a given process [28]. Heat treatments, such as hot isostatic pressing, may be employed to densify the part and alter microstructure for a specific application. A number of other authors have shown HIPing may result in specific microstructures that significantly influence mechanical properties [20, 29]. Here it is demonstrated that in comparison to as-fabricated surfaces, hot isostatic pressing substantially reduced porosity (1.04 to 0.02% - Figure 3) and S_a (34±8 μm to 22±3 μm Figure 4) of Ti-6Al-4V implants manufactured using SLM. When comparing micrographs of AF and HIPed samples, however, the surfaces appear macroscopically similar; both clearly exhibit channels of approximately 100-200 μm produced as a result of the island laser tracking pattern used and partially melted precursor particles were observed across the entire surface area of the top face (Figure 2). These similarities may explain why no significant change in the viability and spreading of MC3T3 cells was observed between AF and HIPed surfaces (Figure 5a and b). Generally, comparable levels of cellular metabolic activity (Figure 6a and b) and cytotoxicity (Figure 6c and d) were demonstrated for these samples. The morphology of MC3T3s on AF and HIP surfaces were comparable to osteoblasts spread on conventionally manufactured Ti-6Al-4V surfaces [30-32].

Surface defects, such as the partially melted Ti-6Al-4V particles seen on the surface of AF and HIP samples (Figure 2), have been demonstrated by other authors to impact properties that would be critical to orthopaedic implants, including fatigue [33, 34]. Confocal micrographs revealed that MC3T3 cells were not able to migrate across partially melted particles, as evidenced by the unpopulated spherical areas observed on AF and HIP surfaces (Figure 5). The large angle between the partially

melted spherical particles and the bulk surface may explain why cells were unable to spread in these areas. For adoption of AM implants in orthopaedic applications that typically experience cyclic loading and would benefit from osseointegration it will be important to: 1) optimise AM fabrication properties to enable continuous powder melting throughout the build [35], and 2) post-process to remove any partially melted particles to both minimise wear debris and maximise the surface area available for tissue integration. AM implant designs that facilitate osseointegration are being explored and typically involve the introduction of interconnected porosity to the bulk structure that is appropriately sized for tissue growth and vascularisation [8, 36, 37]. Traditionally-manufactured porous implant surfaces are already in clinical use to facilitate osseointegration so the general principle has been shown to be of merit. Examples include *Trabecular Metal (*Zimmer) and *Porocoat* (DePuy Synthes). AM has the advantage that surface porosity can be incorporated as part of the initial fabrication rather than as a separate manufacturing step, thus streamlining the process. In addition to increasing implant surface area, lattice structures may be utilised to tailor mechanical properties, which has been used as a strategy to minimise stress shielding [38]. Our previous work has explored the possibility to add functionality to implants by incorporating a secondary phase to deliver a therapeutic payload [10]. In a similar manner to osseointegration strategies, this functionalisation approach requires that additional features be added to the surface. Here, it was found that such a design feature did not influence surface topography (Figures 2-4) and in turn, samples with and without surface holes exhibited similar trends in mammalian and bacterial cell adhesion (Figures 5 and 7). Infiltration of MC3T3 cells into the designed surface hole was visualised using confocal microscopy suggesting that such a feature may eventually facilitate tissue ingrowth and mechanical fixation. Notably, such features would act as localised stress risers and therefore introduction of pore channels to facilitate osseointegration or therapeutic release would need to be balanced against mechanical performance. Furthermore, other authors have demonstrated that staphylococcal biofilms may preferentially accumulate in porous coatings on state-of-the-art Ti-6Al-4V surfaces with a significant increase noted above 15% porosity and/or pores up to 150 μm [39].

Following hot isostatic pressing, sandblasting or polishing was shown to successfully remove partially melted precursor particles (Figure 2). These processes were both shown to significantly reduce S_a values compared with equivalent HIPed parts (Figure 4c), resulting in values comparable to those reported for polished conventionally manufactured Ti-6Al-4V surfaces [40]. While interferometry analysis suggested that all treatments resulted in surfaces that exhibited reproducible S_a values (Figure 4b), microscopy images revealed that sandblasted and polished surfaces were qualitatively not spatially consistent across the entire top surface (Figure 2). This was particularly apparent for polished samples; many sections of the tracks produced, as a result of the island scanning strategy, were still present. It is suggested that these localised areas, which are expected to have exhibited a higher degree of roughness, explain why viable MC3T3 pre-osteoblasts were observed to cluster on these surfaces after 7 days of culture (Figure 5d). Since similar levels of viability, metabolic activity and cytotoxicity were seen on days 1 and 3 between all SLM samples (Figures 5 and 6) it is suggested that the localised rough areas of polished samples supported initial attachment of MC3T3 cells but the mirror-like finish across the rest of the surface area was not conducive to migration and proliferation. This inconsistent surface finishing resulted in a significantly lower Alamar blue reduction and higher LDH cytotoxicity after 7 days of culture (HIP + P compared with HIP). Since only the top surface of SLM parts exhibit the peaks and trough of this fabrication approach, cellular adhesion to other faces is expected to have been minimal. The peaks and troughs of the island scanning strategy were less apparent in sandblasted samples compared with AF and HIP samples, which may explain why similar mammalian cell behaviour was observed on HIP + SB samples compared with HIP + P surfaces. However, viable cells were not observed to cluster on the surfaces of sandblasted parts as seen on polished parts and instead were more randomly distributed (Figure 5). In addition to quantifying S_a, Wennerberg and Albrektsson recommended the use of average spacing between irregularities crossing the mean plane (S_{cx}) and developed surface area ratio (S_{dr}), i.e. a ratio between 3D measurement and a 2D reference plane [41]. While Wennerberg's study was focused on topographical evaluation of screw-type oral implants [41], the

results of this study demonstrate that simultaneous quantification of these three parameters may be particularly useful in evaluating AM implants. Mathematical descriptions of these parameters may be found in the work of Stout *et al.* [42].

It is possible that the parts analysed in this study exhibited different surface chemistries and this may have contributed to changes in cellular behaviour. For example, Vaithilingam *et al.* detected heterogeneity and differences in vanadium concentration on the surfaces of as-fabricated and mechanically polished SLM Ti-6Al-4V parts using X-ray photoelectron spectroscopy [43]. However, Vaithilingham *et al*. concluded that these chemical differences did not influence the viability of seeded fibroblasts assessed by LDH and Live/Dead assays but no cellular functionality testing was performed.

While fewer MC3T3 cells adhered to sandblasted and polished surfaces compared with AF and HIP samples (Figure 5) this trend was not observed for the three investigated bacterial organisms (Figure 7). In the case of some samples (S*taphylococcus aureus* and *epidermidis* – hole; S*taphylococcus aureus* and *Pseudomonas aeruginosa* – no hole) significantly more biofilm formed on HIP + SB implants compared with HIPing alone, however no consistent trends were observed for the crystal violet assay (Figure 7a). This may have been due to the experimental set up, in which bacterial cells could adhere to all available surfaces (i.e. top and curved sides – Figure 1a). In comparison initial seeding and subsequent live/dead staining was only conducted on the top flat surfaces, which were shown to exhibit significantly different S_a values (Figure 4) and more clear differences in bacterial adhesion between surfaces (Figure 7b and c). This highlights the importance of considering any topographical variations in part surfaces which are built in different orientations to the build plate (i.e. top versus side).

Cerca *et al*. demonstrated that clinical isolates of *Staphylococcus epidermidis* adhered to a greater extent on hydrophobic surfaces compared with hydrophilic [44]. Interestingly in this study, confocal z-stacks revealed that initial adhesion of all three bacterial species was more homogeneous and dense for sandblasted samples, which exhibited the lowest contact angle compared with all other surfaces

(Figures 3 and 7c). Therefore, this may suggest that contaminated blast media was embedded onto the SB surfaces, which may have increased the propensity for these surfaces to be colonised. As an aside observation, during contact angle measurements it was noted that the water droplet quickly (< 1 minute) flattened on SB surfaces, which may suggest that it penetrated the AM part. Other authors have reported higher but still hydrophilic, contact angles (55 - 65º) for sandblasted titanium surfaces [45], which may support the assertion that the contact angle reported here (7.90 ± 1.65º) for SB surfaces after 1 minute was skewed due to water penetration. Regardless, these results suggest that sandblasting may put implant surface at greater risk of bacterial adhesion if the blast media is not sufficiently removed.

The adhesion of *Staphylococcus aureus* and *Staphylococcus epidermidis* appeared to preferentially occur on the peaks of laser scanning tracks, *Pseudomonas aeruginosa* was more widely spread across all surface treatments (Figure 7b and c). *P. aeruginosa* is generally considered to be an efficient biofilm forming organism which is able to colonise a wide range of inorganic and organic surfaces [46]. The more even adhesion of this species reflects this capacity of the organism. In the case of the polished implants both staphylococci generally locally adhered to rougher surface defects and few cells were observed on the 'mirror-like' areas. Ploux *et al.* highlighted the complexity of these material/bacteria interactions and demonstrated similar degrees of variation in the effect of surface topography on bacterial responses [47]. The great majority of cells of all three species were viable upon staining with only small numbers of dead cells visible, therefore whilst adhesion patterns differ between surface treatments and species this is not likely to be a reflection of different antimicrobial properties of the material.

This exploratory study demonstrates that different post-processing techniques may present the opportunity to tailor cellular adhesion, perhaps with the view of encouraging or discouraging tissue integration for specific clinical applications. For example, osseointegration of the non-articulating surfaces of joint arthroplasty components would be beneficial, whereas it would be detrimental in

components that are designed to be removed, such as paediatric intramedullary nails. However, the similar behaviour of bacterial cells on these surfaces demonstrates a potential trade-off in this approach; often referred to as the race for the surface [48]. To understand these correlations more fully future studies should be designed to enable multi-regression analysis to be employed [39]. Developing biomaterials able to favour cell adhesion without promoting bacterial adhesion is still a challenge. Furthermore, co-culturing mammalian and bacterial cells to obtain a more accurate representation of *in-vivo* surface competition mains difficult since proliferation of the bacteria may result in unfavourable conditions to sustain osteoblast viability [49]. While the literature concerning the effectiveness of surface topography to modulate bacterial adhesion is variable, some chemical modification approaches have shown promise, including antimicrobial peptide coatings [50-52].

5.0 Conclusions

Here the possibility to alter the surface topography of additively manufactured implants post-manufacture to elicit distinct cellular behaviour was demonstrated. This approach presents the opportunity to tailor implant osseointegration, which may be useful in orthopaedics since the degree of tissue integration may be application and patient specific.

Specifically, as-fabricated and hot isostatically pressed parts manufactured using selective laser melting demonstrated a high degree of pre-osteoblast adhesion and the ability to support proliferation as well as migration. It was highlighted that partially melted Ti-6Al-4V particles on these surfaces should be minimised, which is achievable through manufacturing optimisation, in order to maximise the surface area for tissue adhesion. Contrastingly, significantly fewer osteoblasts were viable on sandblasted and polished AM surfaces after 7 days. Utilising these processes to create bespoke prostheses that are designed to be removed, for example paediatric intramedullary nails, presents a potential new advantage of adopting an additive manufacturing route.

Increasing prevalence of orthopaedic implant infection and the global development of antimicrobial resistance highlights the need to develop implants which prevent bacterial adhesion. Despite the minimal adhesion of osteoblasts to sandblasted and polished surfaces three bacterial organisms commonly associated with orthopaedic infections were still shown to adhere and develop biofilms. While these surfaces were not designed to be antimicrobial these results demonstrate the complexity of engineering 'the race to the surface'. It is concluded that this challenge will likely require a combined physical and chemical approach.

References

1. Hull, C.W., *Apparatus for production of three-dimensional objects by stereolithography*. 1986, Google Patents.
2. Gibson, I., D.W. Rosen, and B. Stucker, *Additive manufacturing technologies*. 2010: Springer.
3. Bertol, L.S., R. Schabbach, and L. Dos Santos, *Dimensional evaluation of patient-specific 3D printing using calcium phosphate cement for craniofacial bone reconstruction.* Journal of biomaterials applications, 2016.
4. Parthasarathy, J., *3D modeling, custom implants and its future perspectives in craniofacial surgery.* Annals of maxillofacial surgery, 2014. **4**(1): p. 9.
5. Horn, D., et al., *Reconstruction of a near-total nasal defect using a precontoured titanium mesh with a converse scalping flap.* Journal of Craniofacial Surgery, 2012. **23**(5): p. e410-e412.
6. Emmelmann, C., et al., *Laser additive manufacturing of modified implant surfaces with osseointegrative characteristics.* Physics Procedia, 2011. **12**: p. 375-384.
7. Wu, S.H., et al., *Porous Titanium-6 Aluminum-4 Vanadium Cage Has Better Osseointegration and Less Micromotion Than a Poly-Ether-Ether-Ketone Cage in Sheep Vertebral Fusion.* Artificial organs, 2013. **37**(12): p. E191-E201.
8. Heinl, P., et al., *Cellular Ti–6Al–4V structures with interconnected macro porosity for bone implants fabricated by selective electron beam melting.* Acta biomaterialia, 2008. **4**(5): p. 1536-1544.
9. Lin, C.Y., et al., *Structural and mechanical evaluations of a topology optimized titanium interbody fusion cage fabricated by selective laser melting process.* Journal of Biomedical Materials Research Part A, 2007. **83**(2): p. 272-279.
10. Cox, S.C., et al., *Adding functionality with additive manufacturing: fabrication of titanium-based antibiotic eluting implants.* Materials Science and Engineering: C, 2016. **64**: p. 407-415.
11. Grimm, T., *User's guide to rapid prototyping*. 2004: Society of Manufacturing Engineers.

12. Williams, J.M., et al., *Bone tissue engineering using polycaprolactone scaffolds fabricated via selective laser sintering.* Biomaterials, 2005. **26**(23): p. 4817-4827.
13. Duan, B., et al., *Three-dimensional nanocomposite scaffolds fabricated via selective laser sintering for bone tissue engineering.* Acta Biomaterialia, 2010. **6**(12): p. 4495-4505.
14. Mullen, L., et al., *Selective Laser Melting: A regular unit cell approach for the manufacture of porous, titanium, bone in-growth constructs, suitable for orthopedic applications.* Journal of Biomedical Materials Research Part B: Applied Biomaterials, 2009. **89**(2): p. 325-334.
15. Van der Stok, J., et al., *Selective laser melting-produced porous titanium scaffolds regenerate bone in critical size cortical bone defects.* Journal of Orthopaedic Research, 2013. **31**(5): p. 792-799.
16. Fukuda, A., et al., *Osteoinduction of porous Ti implants with a channel structure fabricated by selective laser melting.* Acta Biomaterialia, 2011. **7**(5): p. 2327-2336.
17. Ponader, S., et al., *In vivo performance of selective electron beam-melted Ti-6Al-4V structures.* Journal of biomedical materials research Part A, 2010. **92**(1): p. 56-62.
18. Qiu, C., N.J. Adkins, and M.M. Attallah, *Microstructure and tensile properties of selectively laser-melted and of HIPed laser-melted Ti–6Al–4V.* Materials Science and Engineering: A, 2013. **578**: p. 230-239.
19. Van Hooreweder, B., et al., *Improving the fatigue performance of porous metallic biomaterials produced by Selective Laser Melting.* Acta Biomaterialia, 2017. **47**: p. 193-202.
20. Leuders, S., et al., *On the mechanical behaviour of titanium alloy TiAl6V4 manufactured by selective laser melting: Fatigue resistance and crack growth performance.* International Journal of Fatigue, 2013. **48**: p. 300-307.
21. Chan, K.S., et al., *Fatigue life of titanium alloys fabricated by additive layer manufacturing techniques for dental implants.* Metallurgical and Materials Transactions A, 2013. **44**(2): p. 1010-1022.
22. Hollander, D.A., et al., *Structural, mechanical and in vitro characterization of individually structured Ti–6Al–4V produced by direct laser forming.* Biomaterials, 2006. **27**(7): p. 955-963.
23. Zoubos, A.B., S.P. Galanakos, and P.N. Soucacos, *Orthopedics and biofilm—what do we know? A review.* Medical Science Monitor, 2012. **18**(6): p. RA89-RA96.
24. Huang, H.-H., et al., *Effect of surface roughness of ground titanium on initial cell adhesion.* Biomolecular engineering, 2004. **21**(3): p. 93-97.
25. Cox, S.C., et al., *Adding functionality with additive manufacturing: Fabrication of titanium-based antibiotic eluting implants.* Materials Science and Engineering: C, 2016. **64**: p. 407-415.
26. Stalder, A.F., et al., *Low-bond axisymmetric drop shape analysis for surface tension and contact angle measurements of sessile drops.* Colloids and Surfaces A: Physicochemical and Engineering Aspects, 2010. **364**(1): p. 72-81.
27. Shu, R., et al., *Hydroxyapatite accelerates differentiation and suppresses growth of MC3T3-E1 osteoblasts.* Journal of Biomedical Materials Research Part A, 2003. **67**(4): p. 1196-1204.

28. Guo, N. and M.C. Leu, *Additive manufacturing: technology, applications and research needs.* Frontiers of Mechanical Engineering, 2013. **8**(3): p. 215-243.
29. Thijs, L., et al., *A study of the microstructural evolution during selective laser melting of Ti–6Al–4V.* Acta Materialia, 2010. **58**(9): p. 3303-3312.
30. Park, J.-W., et al., *Enhanced osteoblast response to an equal channel angular pressing-processed pure titanium substrate with microrough surface topography.* Acta biomaterialia, 2009. **5**(8): p. 3272-3280.
31. Webster, T.J. and J.U. Ejiofor, *Increased osteoblast adhesion on nanophase metals: Ti, Ti6Al4V, and CoCrMo.* Biomaterials, 2004. **25**(19): p. 4731-4739.
32. Chua, P.-H., et al., *Surface functionalization of titanium with hyaluronic acid/chitosan polyelectrolyte multilayers and RGD for promoting osteoblast functions and inhibiting bacterial adhesion.* Biomaterials, 2008. **29**(10): p. 1412-1421.
33. Greitemeir, D., et al. *Additive Layer Manufacturing of Ti-6Al-4V and Scalmalloyrp© Fatigue and Fracture*. in *27th ICAF Symposium*. 2013.
34. Frazier, W.E., *Metal additive manufacturing: a review.* Journal of Materials Engineering and Performance, 2014. **23**(6): p. 1917-1928.
35. Song, B., et al., *Effects of processing parameters on microstructure and mechanical property of selective laser melted Ti6Al4V.* Materials & Design, 2012. **35**: p. 120-125.
36. Heinl, P., et al., *Cellular titanium by selective electron beam melting.* Advanced Engineering Materials, 2007. **9**(5): p. 360-364.
37. Bandyopadhyay, A., et al., *Application of laser engineered net shaping (LENS) to manufacture porous and functionally graded structures for load bearing implants.* Journal of Materials Science: Materials in Medicine, 2009. **20**(1): p. 29-34.
38. Harrysson, O.L., et al., *Direct metal fabrication of titanium implants with tailored materials and mechanical properties using electron beam melting technology.* Materials Science and Engineering: C, 2008. **28**(3): p. 366-373.
39. Braem, A., et al., *Staphylococcal biofilm growth on smooth and porous titanium coatings for biomedical applications.* Journal of Biomedical Materials Research Part A, 2014. **102**(1): p. 215-224.
40. Deligianni, D.D., et al., *Effect of surface roughness of the titanium alloy Ti–6Al–4V on human bone marrow cell response and on protein adsorption.* Biomaterials, 2001. **22**(11): p. 1241-1251.
41. Wennerberg, A. and T. Albrektsson, *Suggested guidelines for the topographic evaluation of implant surfaces.* International Journal of Oral & Maxillofacial Implants, 2000. **15**(3).
42. Stout, K.J., *Development of methods for the characterisation of roughness in three dimensions*. 2000.
43. Vaithilingam, J., et al., *Surface chemistry of Ti6Al4V components fabricated using selective laser melting for biomedical applications.* Materials Science and Engineering: C, 2016. **67**: p. 294-303.
44. Cerca, N., et al., *Quantitative analysis of adhesion and biofilm formation on hydrophilic and hydrophobic surfaces of clinical isolates of Staphylococcus epidermidis.* Research in microbiology, 2005. **156**(4): p. 506-514.
45. Grubova, I., et al. *Comparative evaluation of the sand blasting, acid etching and electron beam surface treatments of titanium for medical application*. in *Strategic Technology (IFOST), 2016 11th International Forum on*. 2016. IEEE.

46. Masák, J., et al., *Pseudomonas biofilms: possibilities of their control.* FEMS microbiology ecology, 2014. **89**(1): p. 1-14.
47. Ploux, L., A. Ponche, and K. Anselme, *Bacteria/material interfaces: role of the material and cell wall properties.* Journal of Adhesion Science and Technology, 2010. **24**(13-14): p. 2165-2201.
48. Subbiahdoss, G., et al., *Microbial biofilm growth vs. tissue integration:"The race for the surface" experimentally studied.* Acta biomaterialia, 2009. **5**(5): p. 1399-1404.
49. Lee, J.-H., et al., *Effects of Staphylococcus epidermidis on osteoblast cell adhesion and viability on a Ti alloy surface in a microfluidic co-culture environment.* Acta biomaterialia, 2010. **6**(11): p. 4422-4429.
50. Neoh, K.G., et al., *Balancing osteoblast functions and bacterial adhesion on functionalized titanium surfaces.* Biomaterials, 2012. **33**(10): p. 2813-2822.
51. Kazemzadeh-Narbat, M., et al., *Antimicrobial peptides on calcium phosphate-coated titanium for the prevention of implant-associated infections.* Biomaterials, 2010. **31**(36): p. 9519-9526.
52. Gao, G., et al., *The biocompatibility and biofilm resistance of implant coatings based on hydrophilic polymer brushes conjugated with antimicrobial peptides.* Biomaterials, 2011. **32**(16): p. 3899-3909.

Acknowledgements

The authors would like to acknowledge the Engineering and Physical Sciences Research Council (grant number EP/L020815/1) for funding this research.

Disclosures

No conflict of interest is declared.

For Table of Contents Use Only

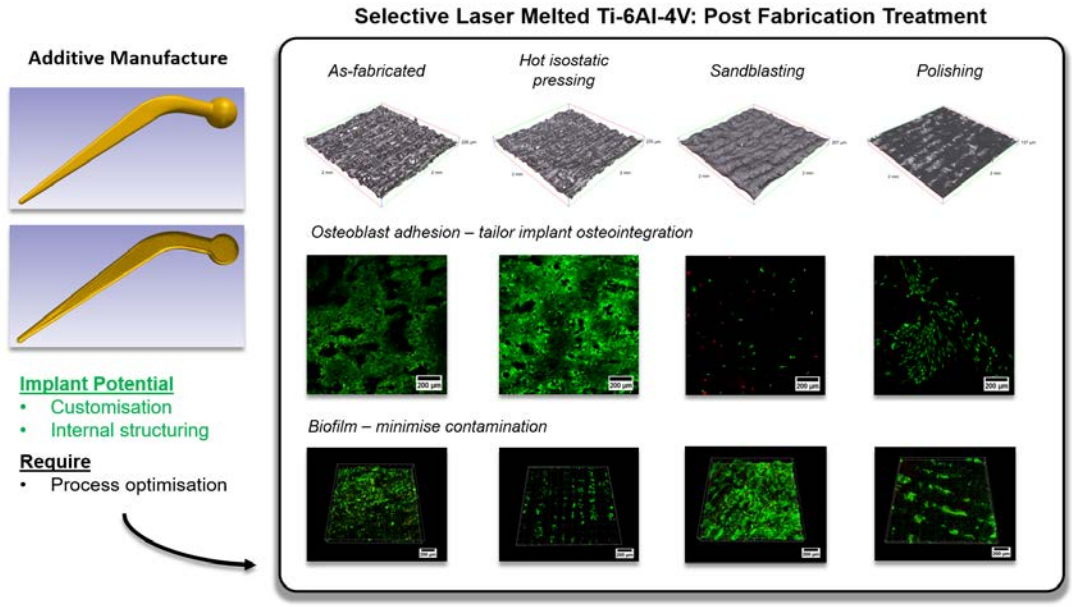

Surface Finish has a Critical Influence on Biofilm Formation and Mammalian Cell Attachment to Additively Manufactured Prosthetics

Sophie C. Cox[1*], Parastoo Jamshidi[2], Neil M. Eisenstein[1,3], Mark A. Webber[4,5], Hanna Burton[1,6], Richard J. A. Moakes[1], Owen Addison[6], Moataz Attallah[2], Duncan E.T. Shepherd[7], Liam M. Grover[1]